UDC 5378(075)

STATISTICAL TEST OF REGULAR BLACK-HOLE GEOMETRY USING HFQPO OBSERVATIONS

Safarov Omadjon Juraboyevich,
Samarkand State University named after Sharof Rashidov, Samarkand, Uzbekistan
omadjonsafarov0305@gmail.com

Abstract. *We test the everywhere-regular branch of a nonlinear-electrodynamic black-hole geometry using twin-peak high-frequency quasi-periodic oscillations (HFQPOs) and independent dynamical-mass information. The exact regular branch imposes $M = q^3/\alpha$, so a common action scale implies a mass-dependent dimensionless deformation. For the adopted three-source relativistic-precession (RP) benchmark, 5000 parametric-bootstrap realizations give $\lambda_{stat} = 0.28388$, a calibrated 68% interval 0.17324-0.42666 and a 95% interval 0.09499-0.59698; the homogeneity statistic is $Q = 0.4864$ with $p_Q = 0.777 \pm 0.006$. The data are compatible with a common static coordinate within the adopted model, but the test has low power and is strongly sensitive to spin, HFQPO provenance, QPO scatter and mass priors. Kerr-generated frequencies can mimic a nonzero static deformation, while alternative mass choices and 0-5% QPO scatter move the fitted value over 0.1138-0.4041. The result is therefore a consistency test of a restricted static surrogate, not a measurement of a universal NED coupling.*

Key words: *regular black hole, nonlinear electrodynamics, HFQPOs, relativistic precession, spin degeneracy, bootstrap.*

HFQPO KUZATUVLARI ASOSIDA REGULAR QORA TUYNUK GEOMETRIYASINI STATISTIK TEKSHIRISH

Annotatsiya. *Maqolada chiziqli bo‘lmagan elektrodinamika asosidagi butun sohada muntazam bo‘lgan qora tuynuk geometriyasining aniq muntazam tarmog‘i yuqori chastotali kvazi-davriy tebranishlar va mustaqil dinamik massa ma’lumotlari yordamida tekshiriladi. Muntazamlik sharti $M = q^3/\alpha$ umumiy harakat parametrida massa bilan bog‘liq o‘lchamsiz deformatsiyani hosil qiladi. Uch manbali relyativistik presessiya modelida $\lambda_{stat} = 0.28388$, 68% bootstrap oralig‘i 0,17324-0,42666, 95% oralig‘i 0,09499-0,59698 va bir jinslilik statistikasi $Q = 0.4864$ ($p_Q = 0.777 \pm 0.006$) olindi. Biroq natija spin, QPO manbasi, QPO tarqoqligi va massa taqsimotiga sezgir. Kerr geometriyasidan hosil qilingan chastotalar statik modelda nol bo‘lmagan deformatsiya sifatida ko‘rinishi mumkin. Shu sababli λ_{stat} fundamental NED bog‘lanish o‘lchovi emas, balki cheklangan statik modelning moslik koordinatasi sifatida talqin qilinadi.*

Kalit so‘zlar: *muntazam qora tuynuk, nochiziqli elektrodinamika, HFQPO, relyativistik presessiya, spin degeneratsiyasi, bootstrap.*

СТАТИСТИЧЕСКАЯ ПРОВЕРКА ГЕОМЕТРИИ РЕГУЛЯРНОЙ ЧЁРНОЙ ДЫРЫ ПО НАБЛЮДЕНИЯМ HFQPO

Аннотация. *Исследуется регулярная ветвь нелинейно-электродинамической геометрии чёрной дыры с помощью двухпиковых высокочастотных квазипериодических осцилляций и независимых динамических оценок массы. Точное условие регулярной ветви $M = q^3/\alpha$ задаёт зависящую от массы безразмерную деформацию при едином масштабе действия. Для принятого трёхисточникового эталона релятивистской прецессии получено $\lambda_{stat} = 0.28388$; бутстреп-интервалы составляют 0,17324-0,42666 (68%) и 0,09499-0,59698 (95%), а статистика однородности $Q = 0.4864$ при $p_Q = 0.777 \pm 0.006$. Результат зависит от спина, происхождения HFQPO, систематического разброса частот и выбора массовых приоров. Следовательно, λ_{stat} следует интерпретировать как координату согласованности в рамках ограниченной статической модели, а не как прямое измерение фундаментальной константы NED.*

Ключевые слова: *регулярная чёрная дыра, нелинейная электродинамика, HFQPO, релятивистская прецессия, спиновая вырожденность, бутстреп.*

Introduction. The replacement of the curvature singularity by a regular core has motivated a broad class of nonsingular black-hole geometries. Regularity, however, is only one requirement: horizon structure,

weak-field behaviour, energy conditions, a consistent matter Lagrangian and dynamical stability must be considered separately [1-4]. Nonlinear electrodynamics (NED) is a particularly developed route because regular magnetic solutions can be obtained within general relativity, while the corresponding effective photon geometry can differ from the background metric [3-5]. The Fan-Wang family provides a compact description containing Maxwellian, Bardeen-like and Hayward-like subclasses [6]. On the everywhere-regular branch, the parameters are not independent: $M = q^3/\alpha$.

This relation is important observationally because one common action scale produces a source-dependent dimensionless deformation. The present work tests this cross-source restriction rather than fitting an unrelated deformation to every black hole. HFQPOs probe the strong-field region of accretion flows. In geodesic interpretations, the observed peaks are related to the orbital and epicyclic frequencies or to combinations such as periastron precession [7-9]. Their usefulness is accompanied by systematic uncertainty: peak identification, disk physics, state dependence and the adopted black-hole mass all affect the inferred geometry. In addition, the three systems used here have nonzero published spin estimates, so a static metric may absorb omitted frame dragging into an apparent deformation [10-12].

We therefore define $\lambda_{stat} = \alpha/M_{\odot}^2$ as a static-equivalent coordinate, not as an unbiased measurement of a fundamental NED coupling. The analysis combines analytic admissibility checks, a profile likelihood for HFQPO and dynamical-mass data, a 5000-realization parametric bootstrap, and sensitivity tests for QPO provenance, spin, mass alternatives and intrinsic QPO scatter. With only three independent source blocks, non-rejection of a common coordinate must be interpreted cautiously.

Regular solution and universal scaling

We use the action convention

$$S = \frac{1}{16\pi}\int d^4x\sqrt{-g}\,[R - \mathcal{L}(F)], \qquad F = F_{\mu\nu}F^{\mu\nu}. \tag{1}$$

For the magnetic configuration, the Fan–Wang metric can be written as

$$ds^2 = -f(r)dt^2 + \frac{dr^2}{f(r)} + r^2 d\Omega^2, \quad f(r) = 1 - \frac{2Mr^{\mu-1}}{(r^\nu+q^\nu)^{\frac{\mu}{\nu}}}. \tag{2}$$

The exact regular branch obeys

$$M = \frac{q^3}{\alpha}. \tag{3}$$

Introducing $x = r/M$, $g = q/M$ and $\lambda = \alpha/M_{\odot}^2$ gives

$$f(x) = 1 - \frac{2x^2}{(x^\nu+g^\nu)^{\frac{3}{\nu}}}, \qquad g_i = \left[\frac{\lambda}{(M_i/M_{\odot})^2}\right]^{\frac{1}{3}}. \tag{4}$$

Thus the same λ produces a larger dimensionless deformation for a lower-mass source. This mass dependence is the central cross-source hypothesis. We consider the Maxwellian, Bardeen-like and Hayward-like subclasses used in the original benchmark. The analysis is restricted to the black-hole region in which a horizon exists.

The horizon is determined by $f(x_h) = 0$; extremality additionally requires $f'(x_h) = 0$. The resulting maximum deformation is subclass dependent. For the three cases used in the source study the quoted limits are 0.2963 (Maxwellian), 0.7698 (Bardeen-like) and 1.0583 (Hayward-like). All fits enforce the relevant horizon bound.

Subclass	g_{ext}	Maxwell optical limit
Maxwellian	0.2963	yes
Bardeen-like	0.7698	no
Hayward-like	1.0583	no

NED perturbations propagate on an effective metric, schematically

$$g_{eff}^{\mu\nu} = \mathcal{L}_{\mathcal{F}}\, g^{\mu\nu} - 4\mathcal{L}_{\mathcal{F}\mathcal{F}}\, F_{\rho}^{\mu}F^{\rho\nu}. \tag{5}$$

For the magnetic solution the effective line element can be written with a modified angular coefficient. The exterior checks performed in the source satisfy the selected sufficient positivity inequalities, but this is not a proof of complete stability in every perturbation sector. Moreover, only the Maxwellian subclass recovers the standard Maxwell optical cone in the stated conformal representation; ordinary EHT shadow likelihoods are therefore not used for the Bardeen-like and Hayward-like timing comparisons.

HFQPO model and observational inputs

For circular timelike motion, the coordinate-time orbital and radial epicyclic frequencies are

$$\Omega_{\varphi}^{2} = \frac{f'}{2r}, \qquad \Omega_{r}^{2} = \frac{1}{3}\left(ff'' - 2f'^{2} + \frac{3ff'}{r}\right). \tag{6}$$

Spherical symmetry gives $\Omega_{\theta} = \Omega_{\varphi}$. Stable circular motion requires $\Omega_{r}^{2} > 0$; the outer root $\Omega_{r} = 0$ defines the ISCO. The observable frequencies scale approximately as M^{-1}, so the independent dynamical-mass likelihood strongly constrains the coupling fit.

We retain three timing prescriptions as model sensitivities. In the RP model, $\nu_{U} = \nu_{\varphi}$ and $\nu_{L} = \nu_{\varphi} - \nu_{r}$. The WD prescription uses combinations of orbital and radial motion, while the ER prescription identifies the peaks directly with the orbital/vertical and radial epicyclic frequencies. Each source has a fitted QPO radius, constrained to a stable circular branch outside the ISCO. These prescriptions are not combined as repeated measurements of one physical parameter.

The baseline observational blocks are:

Source	ν_U (Hz)	ν_L (Hz)	Dynamical mass ($M_{\odot}$)
GRO J1655-40	451 ± 5	298 ± 4	6.3 ± 0.5
XTE J1550-564	276 ± 3	184 ± 5	9.10 ± 0.61
GRS 1915+105	168 ± 3	113 ± 5	13.69 ± 2.0

For compactness, the table follows the adopted source blocks of the original analysis; the GRO upper frequency is 298 Hz and the source pair is treated within the RP likelihood. GRO and XTE have direct RXTE support for the relevant high-frequency features, whereas the 113/168-Hz GRS block is an adopted comparative construction. The original simultaneous GRS pair was 41.5/69.2 Hz, and the literature discussion indicates that the 113-Hz feature is not a direct record in the later analysis [9]. M82 X-1 is excluded because its commonly quoted mass scale is inferred from the same QPO phenomenon and would be circular as an independent validation.

Statistical construction.

For source i, the baseline objective combines the two-frequency residual vector with its covariance and an independent dynamical-mass likelihood:

$$\chi_{i}^{2} = r_{\nu,i}^{T}\, C_{\nu,i}^{-1}\, r_{\nu,i} - 2\ln\mathcal{L}_{M,i}. \tag{7}$$

At fixed λ, both the nuisance mass and QPO radius are reoptimized. For GRS 1915+105, the asymmetric mass uncertainty is represented by a normalized split-normal distribution rather than by averaging the upper and lower errors. The common profile is

$$\chi_{i,\mathrm{prof}}^{2}(\lambda) = \min_{M_i, x_i} \chi_{i}^{2}, \qquad \chi_{\mathrm{common}}^{2}(\lambda) = \sum_{i} \chi_{i,\mathrm{prof}}^{2}(\lambda). \tag{8}$$

The homogeneity statistic compares the optimized common model with a source-specific reference:

$$Q = \min_{\lambda} \sum_{i} \chi_{i,\mathrm{prof}}^{2}(\lambda) \; - \; \sum_{i} \min_{\lambda_i} \chi_{i,\mathrm{prof}}^{2}(\lambda_i). \tag{9}$$

For the main RP fit the source-specific alternative is effectively saturated, so its role is to define a reference minimum rather than a conventional predictive competitor. We therefore do not rank the common and source-specific fits using AIC or BIC.

A 5000-realization parametric bootstrap is generated from the best common-coupling fit. Each realization is refitted under both common and source-specific hypotheses. The bootstrap provides the null distribution of Q, empirical profile thresholds, and a boundary-aware distribution for the $\lambda = 0$ test. This is important because $\lambda = 0$ lies at the physical edge of the parameter space, where standard regular likelihood-ratio asymptotics need not apply [13,14].

Baseline result

For the Maxwellian subclass and RP identification, the fitted common coordinate is

$$\hat{\lambda}_{\mathrm{stat}} = 0.2838763742, \qquad \chi^2_{\mathrm{common}} = 0.4864160, \qquad Q = 0.4864160. \tag{10}$$

Among 5000 bootstrap realizations, 3886 have Q at least as large as the observed value, giving $p_Q = 0.77724$ and a Monte Carlo standard error of about 0.0059. The bootstrap-calibrated profile intervals are 0.17324-0.42666 at 68% and 0.09499-0.59698 at 95%. The corresponding action length scale is $\alpha \approx 786.8\ m$, with a 95% interval of approximately 455-1141 m in the adopted parametrization.

The fitted source masses are approximately 6.211, 9.091 and 13.699 $M_{\odot}$ for GRO, XTE and GRS, respectively, and all fitted QPO radii remain outside the ISCO. The residual pattern shows that the coupling is constrained mainly by consistency between timing-inferred masses and external dynamical-mass measurements rather than by a visibly poor fit to the QPO centroids.

The boundary-aware $\lambda = 0$ calculation finds no exceedance among the 5000 boundary-null realizations; with the plus-one convention the resolved Monte Carlo tail is below 1/5001. Within the misspecified static RP family, this places the zero-deformation boundary beyond the resolved bootstrap tail. It should not be interpreted as evidence for NED, because omitted Kerr spin alone can generate a nonzero apparent static deformation.

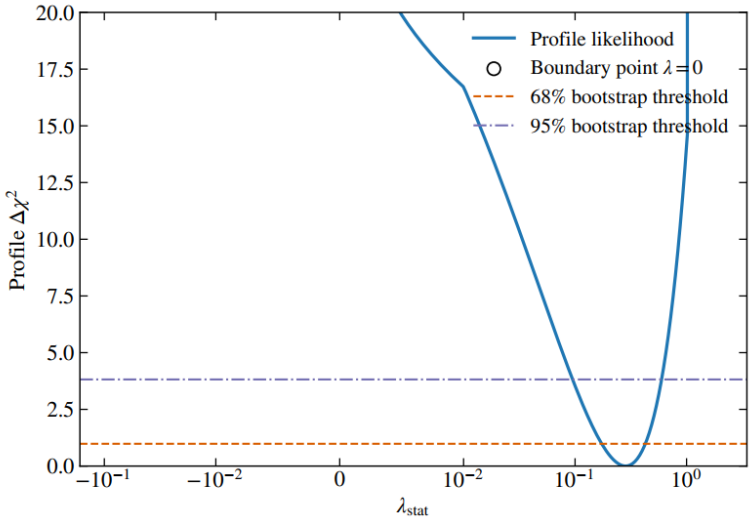


Figure 1. Common profile likelihood with the physical λ = 0 boundary shown explicitly. The solid and dashed horizontal levels are the 68% and 95% bootstrap-calibrated thresholds. The boundary is not represented by an artificial small positive logarithmic value

Sensitivity to QPO provenance and alternative timing models

The evidence construction has a substantial effect. The adopted three-source block gives $\lambda_{stat} \approx 0.2839$ and $Q \approx 0.486$. Using only the more secure GRO+XTE blocks gives $\lambda_{stat} \approx 0.3037$ with a much smaller heterogeneity statistic, but only two independent source blocks remain. Replacing the adopted GRS 113/168-Hz block by the original simultaneous 41.5/69.2-Hz pair moves the optimum to $\lambda_{stat} \approx 0.0941$ and produces strong common-versus-source-specific tension. Adding 5% phenomenological QPO scatter reduces, but does not remove, this tension.

Data construction	λ_{stat}	Q
Adopted 3-source block	0.2839	0.486
GRO + XTE only	0.3037	≈0.011
Original GRS 41.5/69.2 Hz	0.0941	≈55.3
Original GRS pair + 5% scatter	0.1192	≈25.3

The WD fits remain affected by horizon, stability or orbital-domain boundaries, while the ER identification produces systematic mass and lower-frequency residuals under the adopted static family. These results are reported as model sensitivities, not as a ranking of QPO prescriptions.

We also repeat the bootstrap after adding fractional QPO scatter in quadrature. The fitted central value changes only modestly, but the intervals widen: at 1%, 3% and 5% scatter the approximate 68% intervals become 0.1689-0.4332, 0.1524-0.4564 and 0.1362-0.4757, respectively. The corresponding 95% intervals

widen to 0.0883-0.6162, 0.0743-0.6563 and 0.0513-0.7329. Thus formal centroid errors alone can substantially understate uncertainty when percent-level intrinsic variability is admitted.

Kerr-spin confounding

To isolate omitted-spin bias, synthetic RP pairs are generated in Kerr spacetime at the adopted dynamical masses and then fitted with the static Fan-Wang model. For prograde equatorial motion, the Kerr frequencies depend on the dimensionless spin a* and the radius. The radius is fixed by the Kerr frequency ratio rather than chosen arbitrarily, so the test directly measures how a rotating signal can be absorbed by a static surrogate.

A zero-spin control returns $\lambda_{stat} \approx 0$. Timing-informed moderate spins (0.29, 0.34, 0.70 for GRO, XTE and GRS) yield a common apparent $\lambda_{stat} \approx 0.1626$ with $Q \approx 6.77$. A higher-spin spectral set (0.70, 0.76, 0.98) cannot be represented coherently by the static model; the common residual becomes of order 1.8×10^{4}. The latter is a model-failure diagnostic rather than a coupling estimate.

The key implication is a continuous spin-deformation degeneracy: a Kerr signal with nonzero spin can be fitted by a nonzero static deformation even when no NED parameter generated the data. At sufficiently high spin the static family instead ceases to mimic the Kerr frequencies. Consequently, the narrow bootstrap interval around the baseline λ_{stat} is a statistical interval conditional on the static model and does not represent physical uncertainty in a fundamental NED coupling.

Dynamical-mass sensitivity and physical interpretation

Because two QPO frequencies and a fitted radius nearly determine a timing mass, λ_{stat} is identified largely through comparison with the external dynamical-mass likelihood. Replacing the baseline mass choices by alternative published light-curve/evolutionary solutions moves the fitted coordinate. Combined with 0-5% QPO scatter, the source analysis spans approximately

$$0.1138 \leq \lambda_{stat} \leq 0.4041. \tag{11}$$

This range should be read as a model/data-choice envelope, not as a combined confidence interval. Different dynamical-mass determinations rely on different assumptions about light curves, inclination, distance and rotational broadening. Likewise, published spin estimates are model dependent. Without a rotating solution derived from the same NED action, combining spin and λ_{stat} in a single posterior would create artificial precision.

The astrophysical interpretation of the exact branch also remains conditional. A complete model would need a mechanism by which stellar collapse can generate the required conserved magnetic-type charge and by which subsequent accretion preserves the exact relation $M = q^3/\alpha$. The present analysis does not provide such a formation or accretion mechanism.

The optical sector is similarly conditional. If observed photons are perturbations of the same NED field, they follow the effective metric; if the NED stress tensor acts as an effective matter sector while photons are minimally coupled Maxwell fields, they follow the background metric. The action considered here does not select between these possibilities. For that reason, no ordinary EHT shadow likelihood is used to strengthen the stellar-mass timing inference.

Discussion and conclusion

The analysis tests a precise cross-source restriction generated by the exact regular branch: one action parameter must produce a mass-dependent deformation in different black-hole binaries. For the adopted three-source RP construction, the best common coordinate is $\lambda_{stat} = 0.28388$, with bootstrap-calibrated 68% and 95% intervals of 0.17324-0.42666 and 0.09499-0.59698, respectively. The homogeneity statistic $Q = 0.4864$ gives $p_Q = 0.777 \pm 0.006$ under the stated bootstrap null. These numbers describe the internal consistency of the restricted static model. Several qualifications are essential. The GRS 113/168-Hz block is less secure than the GRO and XTE inputs; the simultaneous 41.5/69.2-Hz pair changes the inferred coordinate and increases cross-source tension. Adding 1-5% QPO scatter broadens the intervals. Alternative mass priors move the point estimate, and Kerr-generated frequencies demonstrate that omitted spin can mimic a nonzero static deformation or invalidate the static surrogate at higher spin.

Therefore the result is not a measurement of universal nonlinear-electrodynamic physics. It is a reproducible consistency benchmark for a restricted, static, geodesic timing model. A more decisive test requires a self-consistent rotating solution of the same NED action, observation-level HFQPO likelihoods with trial-aware selection effects, source-specific covariance information, coherent mass and spin modelling, and additional systems with independent dynamical mass measurements. The branch relation $M = q^3/\alpha$ nevertheless provides a clear, falsifiable cross-mass hypothesis for future work.

Mass-prior and identifiability checks

The role of the dynamical-mass prior can be seen directly from the scaling of the geodesic frequencies. For a fixed dimensionless radius and deformation, all characteristic frequencies carry an overall M^{-1} factor. Consequently, the timing pair alone can trade mass against radius, while the external dynamical measurement breaks much of this degeneracy. This is why the fitted λ_{stat} should not be interpreted as being determined by the HFQPO centroids alone.

The baseline analysis uses the adopted GRO, XTE and GRS dynamical masses. The source study also considered alternative published solutions, including the Beer-Podsiadlowski treatment for GRO J1655-40, the Orosz et al. solution for XTE J1550-564 under a different constraint, and an older GRS mass estimate. These alternatives change the balance between timing-inferred and externally measured masses. In combination with the QPO-scatter stress tests, they move the optimum through the broad envelope 0.1138-0.4041.

Because the alternative mass determinations are not statistically independent measurements of one common quantity with a shared likelihood, the envelope is reported descriptively. It should not be compressed into a single error bar. The same caution applies to published spin measurements: timing, continuum and reflection analyses use different physical assumptions. A future joint analysis would need the full likelihoods rather than combining quoted central values and errors after the fact.

Interpretation of the common-coupling test

The homogeneity statistic is designed to answer a restricted question: does forcing the exact branch relation to use one common λ impose a penalty that is unusually large relative to source-specific fits? In the adopted benchmark the observed Q is small compared with most of the bootstrap distribution, so the data construction is compatible with the common static coordinate. However, compatibility is not identification. With only three source blocks, many physically different models can map into a similar range of timing frequencies, and the bootstrap cannot create information that is absent from the sample.

The power limitation is especially important. The secure-only GRO+XTE construction gives a point estimate close to the three-source baseline but has only two independent blocks, so it is poorly suited to a strong cross-source homogeneity test. Conversely, the GRS replacement by the simultaneous 41.5/69.2-Hz pair creates substantial tension. The contrast demonstrates that the statistical conclusion is conditional on which HFQPO features are regarded as the relevant observables.

The same issue appears in the boundary test. The $\lambda = 0$ member lies outside the resolved bootstrap tail within the static RP family, but the Kerr-to-static experiment demonstrates that omitted spin can generate a nonzero λ_{stat} without any NED deformation. Thus a rejection of the static zero-deformation member is a statement about the adequacy of that restricted surrogate, not a direct discrimination between general relativity and nonlinear electrodynamics.

Conditional optical implications

The NED effective metric provides an additional conceptual distinction that is easy to lose in a timing-only fit. Massive particles used in the HFQPO calculation follow the background spacetime metric. Electromagnetic perturbations of the nonlinear field, in contrast, follow the effective characteristic metric. Therefore a photon-ring or shadow prediction depends on which field is identified with the observed radiation.

Compact summary of systematic effects

Source of sensitivity	Effect on λ_{stat} / interpretation
HFQPO provenance	$113/168 - Hz$ GRS block gives 0.2839; $41.5/69.2 - Hz$ replacement gives ≈ 0.0941 and strong tension.
QPO scatter	Central value changes modestly; 95% interval broadens from ≈ 0.597 to ≈ 0.733 at 5% scatter.
Spin omission	Moderate Kerr spins can mimic nonzero static deformation; high spin can make the static surrogate fail.
Mass alternatives	Published mass choices contribute to the broad $0.1138 - 0.4041$ model/data envelope.
Photon sector	Effective NED and minimally coupled Maxwell photons need not follow the same null cones; no EHT likelihood is used.

The source analysis estimates only an illustrative scale for the resulting shadow-radius correction over the fitted stellar-mass λ_{stat} interval and does not use those numbers in the likelihood. Even if the correction is numerically small for the considered extrapolation, the inference would still require transferring a static-equivalent stellar-mass coordinate to supermassive black holes. Such a transfer is not established by the

present model, especially because λ_{stat} is spin-confounded. The optical calculation is therefore a consistency check on the geometry, not an additional observational constraint.

REFERENCES:

1. *I. Dymnikova, "Vacuum nonsingular black hole," Gen. Relativ. Gravit. 24, 235 (1992).*
2. *E. Ayón-Beato and A. García, "Regular black hole in general relativity coupled to nonlinear electrodynamics," Phys. Rev. Lett. 80, 5056 (1998).*
3. *K. A. Bronnikov, "Regular magnetic black holes and monopoles from nonlinear electrodynamics," Phys. Rev. D 63, 044005 (2001).*
4. *C. Moreno and O. Sarbach, "Stability properties of black holes in self-gravitating nonlinear electrodynamics," Phys. Rev. D 67, 024028 (2003).*
5. *M. Novello et al., "Geometrical aspects of light propagation in nonlinear electrodynamics," Phys. Rev. D 61, 045001 (2000).*
6. *Z.-Y. Fan and X. Wang, "Construction of regular black holes in general relativity," Phys. Rev. D 94, 124027 (2016).*
7. *R. A. Remillard and J. E. McClintock, "X-Ray Properties of Black-Hole Binaries," Annu. Rev. Astron. Astrophys. 44, 49 (2006).*
8. *A. Ingram and S. Motta, "A review of quasi-periodic oscillations from black hole X-ray binaries: observation and theory," New Astron. Rev. 85, 101524 (2019).*
9. *T. E. Strohmayer, "Discovery of a Second High-Frequency Quasi-periodic Oscillation from the Microquasar GRS 1915+105," Astrophys. J. Lett. 554, L169 (2001).*
10. *S. E. Motta et al., "Precise mass and spin measurements for a stellar-mass black hole through X-ray timing: the case of GRO J1655–40," Mon. Not. R. Astron. Soc. 437, 2554 (2014).*
11. *S. E. Motta et al., "Black hole spin measurements through the relativistic precession model: XTE J1550-564," Mon. Not. R. Astron. Soc. Lett. 439, L65 (2014).*
12. *J. M. Miller et al., "The Spin of the Near-Extreme Kerr Black Hole GRS 1915+105," Astrophys. J. 652, 518 (2006).*
13. *H. Chernoff, "On the Distribution of the Likelihood Ratio," Ann. Math. Stat. 25, 573 (1954).*
14. *S. G. Self and K.-Y. Liang, "Asymptotic Properties of Maximum Likelihood Estimators and Likelihood Ratio Tests under Nonstandard Conditions," J. Am. Stat. Assoc. 82, 605 (1987).*
15. *J. A. Orosz, J. F. Steiner, J. E. McClintock et al., "An improved dynamical model for the microquasar XTE J1550-564," Astrophys. J. 730, 75 (2011).*